1

Image and Imaging System Characteristics

1.1 General Image and Imaging System Characteristics

A clinical diagnosis may require radiological scans from multiple imaging modalities. For example, a patient may have an exploratory ultrasound followed by some combination of CT, MRI, and/or PET. Each of these modalities provides different types of clinical information (anatomical and/or functional, static and/or dynamic) which together give as complete as possible an "inside view" of what is happening in the body. Some of these modalities such as ultrasound are point-of-care, which means that small portable units can be used relatively easily, quickly, and cheaply: others are very expensive, large, and heavy fixed-site systems which might require the patient to wait several weeks before an appointment is available.

In addition to the different types of information provided, each of the modalities also has specific image characteristics: these include intrinsic differences in spatial resolution (from the low micrometer range for OCT to several millimeters for SPECT), as well as signal-to-noise ratio (SNR) and contrast-to-noise ratio (CNR). Over several decades there have been constant technological improvements in imaging hardware and image processing algorithms which have led to enormous increases in the performance and diagnostic quality of clinical scans from each of the modalities covered in this book. Quantitatively, we can evaluate system performance via the three basic measures of spatial resolution, SNR, and CNR (taking into account the scan time required) [1–7]. There is a strong interdependence between these three measures, in terms of the parameters and hardware used to acquire and process the images. For optimal system design and analysis it is very important to understand the relationship between these measures, and also to realize that this relationship depends on which particular imaging modality is being considered. This chapter covers several of the quantitative aspects of assessing image quality, some of the trade-offs between SNR, CNR, and spatial resolution, and a basic description of data acquisition principles which are common

Introduction to Biomedical Imaging, Second Edition. Andrew Webb.

Companion website: www.wiley.com/go/webb2e

to all of the digital data acquired, processed, and stored by modern clinical imaging modalities.

1.2 Concept of Spatial Frequency

The concept of spatial frequency is very useful in characterizing the performance of an imaging system. The spatial frequency modulation transfer function (MTF), covered later in this chapter, is one of the key manufacturer specifications for many different components of a system. As a simple example of spatial frequency, consider a series of black lines on a white background, as shown in Figure 1.1a–c. The spatial frequency, k, is defined as the number of lines/mm in a particular dimension, x, y, or z. The closer together the lines, the higher the spatial frequency, and the greater must be the resolving power of an imaging system in order to produce an image in which the lines are distinct. This concept can be extended to multiple dimensions, as shown in Figure 1.1d, with the object characterized by spatial frequencies, k_x and k_y, in this case.

Obviously, the body does not consist of regularly spaced structures such as those shown in Figure 1.1, but rather the locations and geometries of specific organs and structures within these organs correspond to a range of spatial frequencies. Take for example an MRI of the head as shown in Figure 1.2a. In this particular image, there are different signal intensities from subcutaneous fat (bright), bone (zero), cerebrospinal fluid (bright), and white and gray matter (intermediate). A plot of the signal intensity in one dimension (along the dotted line) shows that there are

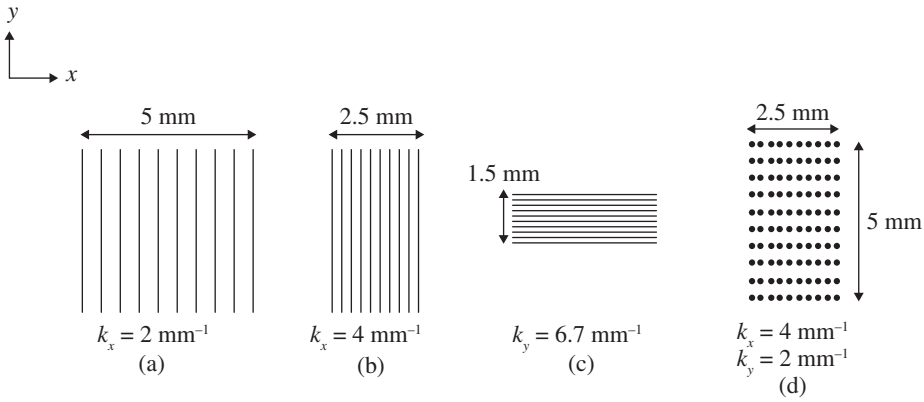

Figure 1.1 Illustration of spatial frequency. (a–c) The object to be imaged consists of ten narrow lines with different separations in either the x- or y-dimension. The respective k-value is given in units of lines/mm, or more commonly mm^{-1}. (d) For a two-dimensional object the corresponding parameters are k_x and k_y.

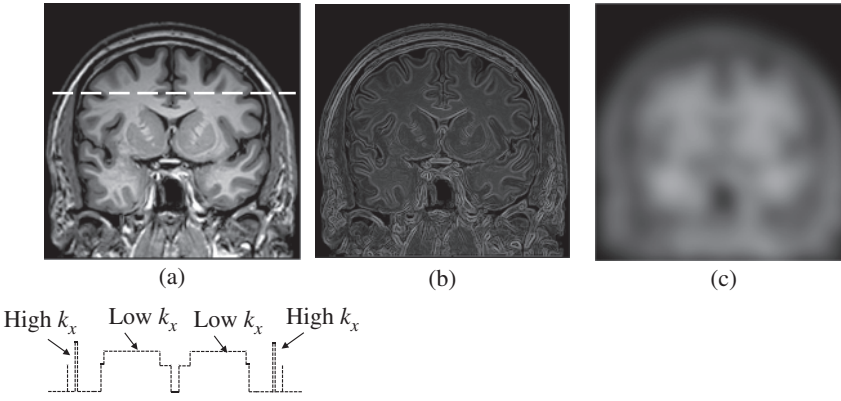

Figure 1.2 (a) An MRI of the head, showing many different tissues in the brain and skull. The line plot below the image shows the projection of the signal intensity along the dotted line. Areas where the signal intensity changes rapidly represent high k_x values, and regions of relatively uniform signal intensity correspond to low k_x values. (b) A map of areas which correspond to high k_x and k_y values. (c) A map of areas corresponding to low k_x and k_y values.

regions of the brain where the signal changes rapidly as a function of x-coordinate (corresponding to high k_x values) and other regions where there is very little change (low k_x values). Figure 1.2b shows the areas corresponding to high k_x values, and Figure 1.2c those corresponding to low k_x values. These two images illustrate the important point that sharp edges and small features are represented by high spatial frequencies, and areas of slowly varying contrast by low spatial frequencies. It might seem, therefore, that we want to design an imaging system which is very sensitive to high spatial frequencies, so that we can detect very small pathologies. However, we also have to consider that every image contains noise, which is randomly distributed across the image. The value of this noise changes rapidly from pixel to pixel, and so random noise corresponds to very high spatial frequencies. Therefore, an imaging system, or an image processing algorithm, which can capture high spatial frequencies, is able to resolve small features in the patient, but is also sensitive to noise. We will return to this point when considering trade-offs between different image characteristics in Section 1.3.

1.3 Spatial Resolution

There are a number of measures which are used to describe the spatial resolution of an imaging modality: the most common are the point spread function (PSF) in the spatial domain and the MTF in the spatial frequency domain.

1.3.1 Imaging System Point Spread Function

The concept of the PSF of a particular imaging system is simply explained by considering a very small "point source" positioned within the imaging field of view (FOV), as shown in Figure 1.3a. This point source could be a small sphere of water for MRI, a small reflector for ultrasound, or a sphere filled with a γ-ray emitter for nuclear medicine. The image of the point source produced by the system could be a very good approximation to the actual object, as shown in Figure 1.3b, it could be blurred in all three dimensions as in Figure 1.3c, or could be blurred primarily in only one dimension as in Figure 1.3d, depending upon the particular imaging modality and how the image was acquired and processed.

The mathematical relationship between the reconstructed image, $I(x, y, z)$, and the object, $O(x, y, z)$, can be represented by:

$$I(x, y, z) = O(x, y, z) * h(x, y, z) \tag{1.1}$$

where * represents a numerical convolution (see Appendix 1.A.3), and $h(x, y, z)$ is the three-dimensional PSF. In a perfect imaging system, the PSF would be a delta function in all three dimensions, and in this case the image would be an exact representation of the object. In practice, the PSF has a finite width, which may be different in the x-, y-, and z-directions, which results in image blurring. The PSF may also contain side lobes, as covered in Chapter 4 on ultrasound.

There are several components which contribute to the overall PSF of an imaging system. The first is the intrinsic physics involved in the imaging method. For example, in Chapter 3 we will see that the γ-rays detected in PET arise from a positron–electron annihilation which occurs at a position with an associated "sphere of uncertainty" of ~1–2 mm. This means that $h(x, y, z)$ due to this process alone represents a sphere with the corresponding dimensions. Second, each component of the detection system, e.g. the lens or charge-coupled device (CCD) camera in an optical imaging device, or the flat panel detector used for computed tomography, also has an associated PSF. Third, we can choose how fine a stepsize

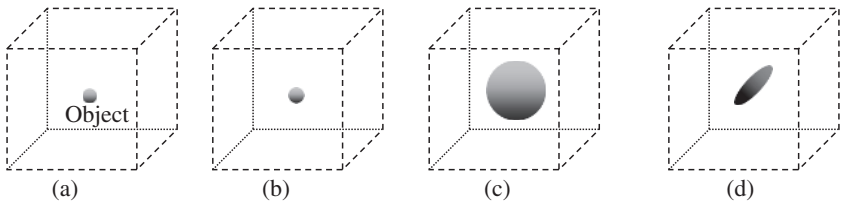

Figure 1.3 (a) The object to be imaged is a very small sphere, termed a point source. (b) An image acquired with a system that has a very narrow PSF: the image is an excellent representation of the actual object. (c) An image with a broad PSF in all three dimensions, resulting in an image which is very blurred. (d) An image with a broad PSF in one dimension and a narrow one in the other two dimensions.

to use to collect the data: this is the sampling contribution to the PSF. The finer the stepsize, the better the spatial resolution, but the longer the scan takes to acquire. The final contribution comes from the image reconstruction algorithm and any subsequent image filtering. Overall the total system PSF, $h_{\text{total}}(x, y, z)$, is given by a series of mathematical convolutions of the individual PSFs for each stage:

$$h_{\text{total}}(x,y,z) = h_{\text{physics}}(x,y,z)^* h_{\text{detector}}(x,y,z)^* h_{\text{sampling}}(x,y,z)^* h_{\text{filter}}(x,y,z) \tag{1.2}$$

A second commonly specified measure of spatial frequency, particularly for flat panel detectors used in CT, is the line spread function (LSF). As the name suggests, this corresponds to a measure which reduces the dimensionality of the three-dimensional PSF to a one-dimensional LSF. Mathematically, the LSF is given by:

$$\text{LSF}(x) = \int \text{PSF}(x,y,z)\text{d}y\text{d}z \tag{1.3}$$

An edge spread function (ESF) is also sometimes defined, where this is defined as the convolution of the LSF with a step function. Experimentally, it is measured using a block of material with a sharp edge.

1.3.2 Imaging System Resolving Power

From a practical point of view the spatial resolution of an image can be defined as the smallest physical distance between two point sources for which the sources can be resolved as being separate. There are two mathematical functions, a sinc or Gaussian, which are good approximations to the LSF in several imaging modalities. If the LSF is a sinc function, then the Rayleigh criterion [8] can be applied, which states that two point sources can be resolved if the peak intensity of the LSF from one source coincides with the first zero-crossing point of the LSF of the other, as shown in Figure 1.4a. In this case the spatial resolution is defined as one-half the width of the central lobe of the sinc function.

If the LSF is a Gaussian function, then the one-dimensional PSF, $h(x)$, can be written as:

$$\text{LSF}(x) = \frac{1}{\sqrt{2\pi\sigma^2}} \exp\left(-\frac{(x-x_0)^2}{\sigma^2}\right) \tag{1.4}$$

where σ is the standard deviation of the distribution and x_0 is the center of the function. The full-width-half-maximum (FWHM) of a Gaussian function is given by:

$$\text{FWHM} = 2\sigma\sqrt{2\ln 2} = 2.36\sigma \tag{1.5}$$

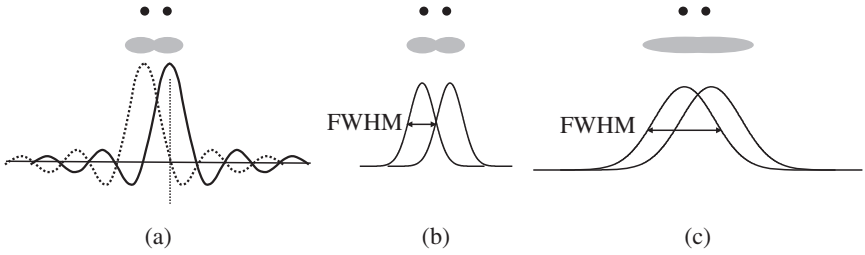

Figure 1.4 (a) For a sinc LSF, the signals from two point sources can be resolved when the separation between them is less than half the width of the main lobe of the sinc function. (b) For an arbitrary LSF, the two point sources can be resolved when their separation is less than the FWHM of the function. (c) In this example the two point sources can no longer be resolved due to the broad FWHM of the LSF.

Therefore, if the separation between the two structures in the x-dimension is greater than 2.36 times the standard deviation of the Gaussian LSF of the imaging system, then the two structures can be distinguished.

If the form of the LSF cannot be described by an analytical function, then it can still be characterized in terms of its FWHM, as shown in Figure 1.4b,c. Then the criterion for resolution is that if the two points sources are separated by a distance greater than the FWHM, they can be resolved.

1.3.3 Imaging System Modulation Transfer Function

The spatial resolution of a system is also often characterized in terms of its MTF, which is measured in the spatial frequency domain. Since the spatial frequency and the spatial domains are related by the Fourier transform (see Appendix 1.A), the MTF and the PSF are mathematically related by:

$$\mathrm{MTF}(k_x, k_y, k_z) = \int_{-\infty}^{\infty} \mathrm{PSF}(x, y, z) e^{-j2\pi k_x x} e^{-j2\pi k_y y} e^{-j2\pi k_z z} dx dy dz \tag{1.6}$$

A "perfect" imaging system would exactly reproduce features corresponding to both low and high spatial frequencies, and would have an MTF of unity for all values of k, as shown in Figure 1.5a. This corresponds to a delta function for the PSF. The effects of different one-dimensional MTFs and corresponding PSFs are shown in Figure 1.5b,c: as expected, via the Fourier transform relationship, a narrow MTF corresponds to a broad PSF and vice versa. As outlined previously, calculation of the overall PSF of an imaging system involves the mathematical convolution of the PSFs from each of the individual components of that system. In the spatial frequency domain, the individual MTFs are multiplied together to give the overall system MTF.

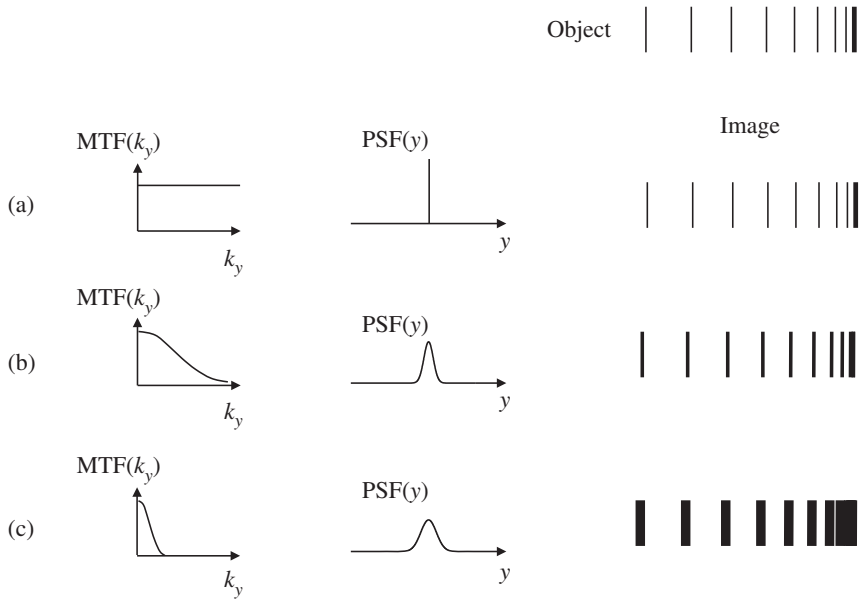

Figure 1.5 (top right) The object being imaged corresponds to a set of lines with increasing spatial frequency from left to right. (a) An ideal MTF and the corresponding PSF produce an image which is an exact representation of the object. (b) A narrower MTF cannot accurately represent the very high spatial frequency information, and the resulting image is slightly blurred. (c) An even narrower MTF "loses" more of high spatial frequency information and produces an image which is more blurred.

1.4 Signal-to-Noise Ratio

The second key characteristic of an image is the SNR: if the value is too low then small features may not be visible, and the degree of confidence of any clinical diagnosis is reduced. The simplest way to measure SNR for a given region-of-interest (ROI) in the image is to calculate the mean of the signal intensity within the ROI, and to divide this by the standard deviation of the noise in a background region which lies outside the body, as illustrated in Figure 1.6a,b:

$$\mathrm{SNR} = \frac{\mu_{\mathrm{ROI}}}{\sigma_{\mathrm{background}}} \tag{1.7}$$

This simple expression assumes that the noise is distributed uniformly over the image. If this is not the case, then an alternative method to estimate the SNR is to run a scan a number of times in succession and to calculate the mean and standard deviation of the signal within the ROI: this is obviously not really feasible for clinical scans, but can be performed in phantoms.

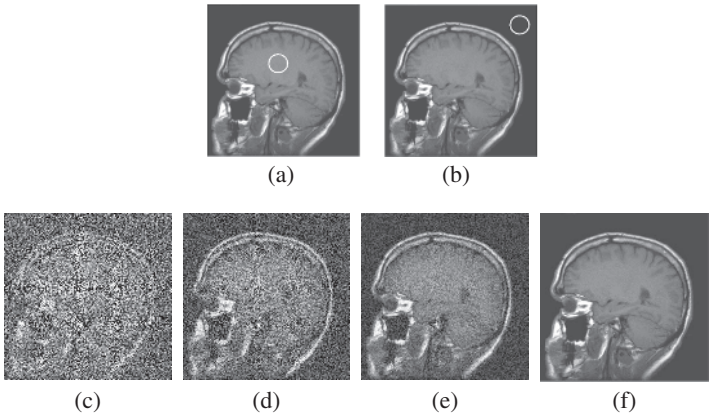

Figure 1.6 (top row) Measurement of SNR in an MRI of the brain estimated by the ratio of (a) the mean signal intensity from all of the voxels within a circular ROI to (b) the standard deviation of the noise from an ROI outside the head. (bottom row) Illustration of signal averaging to improve the image SNR. (c) MRI acquired in a single scan, (d) two identical scans averaged together, (e) four scans, and (f) sixteen scans.

If the SNR from a single scan is too low for a clinical diagnosis, then averaging of multiple scans can be used to increase its value. This process assumes that the signal from successive images is coherent (deterministic), and the noise is incoherent. This procedure of signal averaging is an integral component of OCT, and is also often used in MRI. If the measured signal, $\widehat{S}$, is represented as:

$$\widehat{S} = S + N \tag{1.8}$$

where S is the true signal and N is the noise component with a mean value of zero and a standard deviation σ_{N}, then the SNR for a single scan, $\mathrm{SNR}_{1,}$ is given by:

$$\mathrm{SNR}_1 = \frac{|S|}{\sigma_{\mathrm{N}}} \tag{1.9}$$

If K measurements are acquired and then averaged together, the averaged measured signal, S_K, is given by:

$$S_K = S + \frac{1}{K}\sum_{k=1}^{K} N_k \tag{1.10}$$

The SNR for the averaged scans, SNR_K, is given by:

$$\mathrm{SNR}_K = \frac{|S|}{\sqrt{\mathrm{var}\left\{\frac{1}{K}\sum_{k=1}^{K} S + N_k\right\}}} = K\frac{|S|}{\sigma_{\mathrm{N}}} = SNR_1\sqrt{K} \tag{1.11}$$

Equation (1.11) shows that the SNR is proportional to the square root of the number of averaged images. The trade-off in signal averaging is the increased data acquisition duration, which is K-times as long. Figure 1.6c–f shows the effects of signal averaging for an MRI of the brain.

1.5 Contrast-to-Noise Ratio

Even if the image has a very high SNR, it may not be diagnostically useful unless there is sufficient CNR to distinguish between healthy and pathological tissues. The image contrast, C_{AB}, between two tissues A and B is defined as:

$$C_{AB} = |S_A - S_B| \tag{1.12}$$

where S_A and S_B are the image intensities from tissues A and B, respectively. The CNR, CNR_{AB}, between tissues A and B is defined in terms of their respective SNRs:

$$\mathrm{CNR}_{AB} = \frac{C_{AB}}{\sigma_\mathrm{N}} = \frac{|S_A - S_B|}{\sigma_\mathrm{N}} = |\mathrm{SNR}_A - \mathrm{SNR}_B| \tag{1.13}$$

where σ_N is the standard deviation of the noise. Figure 1.7 illustrates how a decrease in the CNR of an image can result in small features no longer being visible. This can occur either due to a poor SNR as shown in Figure 1.7a–c, or due to a poor spatial resolution as shown in Figure 1.7d–f.

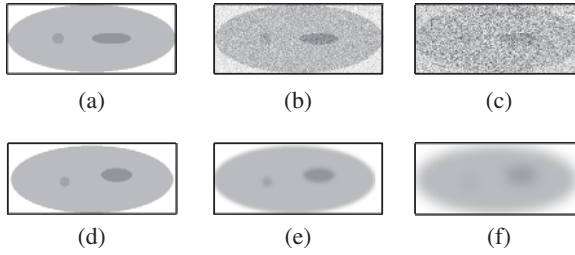

Figure 1.7 Images showing the effect of the CNR on the detectability of two internal features (a–c) illustration of the effects of a decrease in the CNR due to lower SNR. (d–f) The effects on CNR due to poorer spatial resolution.

1.6 Signal Digitization: Dynamic Range and Resolution

In all of the imaging modalities covered in this book, the output of the image detector is an analog electrical signal (current or voltage), which first passes through a low noise amplifier and is then digitized by an analog-to-digital

converter (ADC). The ADC is characterized by several parameters, the most important of which are its voltage range, resolution, and sampling rate. For example, an ADC for MRI might have a voltage range of +10 to −10 V, a resolution of 16-bits, and a sampling rate of 100 mega samples per second. In terms of resolution, the number of different output levels for an N-bit ADC is given by 2^N, e.g. a 14-bit ADC has 16384 levels. The corresponding voltage resolution (also termed the least significant bit) of the ADC is defined as one-half of the maximum voltage divided by the number of levels. A higher resolution enables more accurate representation of the analog signal, but no matter how high the resolution of the ADC, there is an intrinsic error associated with digitizing an analog signal: this difference is called the quantization error or quantization noise. The higher the ADC resolution, the lower the quantization noise, as shown in Figure 1.8.

There are four different basic types of ADC: flash, successive approximation register, pipelined, and delta-sigma. These architectures each have different properties in terms of their maximum resolution and sampling rate. Flash has very fast sampling (>1 GHz) but relatively low resolution, pipelined and SAR cover an intermediate range, and delta-sigma has very high resolution but lower sampling rates.

After signal digitization, image reconstruction, and any image filtering (See Section 1.7), the images are stored digitally but must also be made available for the physician to view. The viewing station has a certain dynamic range in terms of the number of graytone levels that it can display. Typically the image is displayed at 8-bit resolution, i.e. with 256 different gray levels. Rather than compress the full dynamic range of the digitized image to this resolution, which would lose information, a "window" within the full dynamic range of the data is chosen, and this window is expanded or compressed into the 256 graytone levels that are displayed.

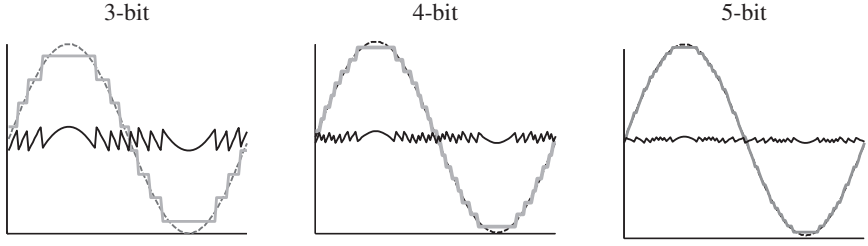

Figure 1.8 A demonstration of the effects of the number of bits on the quantization noise of a digitized signal. The dotted line represents the analog signal, the solid gray line the digital output, and the solid black line the quantization noise. The vertical axis represents amplitude and the horizontal axis time.

1.7 Post-acquisition Image Filtering

After the raw data have been digitized and the images reconstructed, different filters can be applied to improve the image SNR or spatial resolution, or to highlight features such as edges/boundaries between tissues. Since these filters are applied to stored digital data, the effects of different filters can be evaluated without affecting the raw data.

The simplest method to improve SNR is to apply a low-pass filter to the image. The term "low-pass" refers to the characteristics of the filter in the spatial frequency domain, i.e. this type of filter amplifies the low spatial frequencies in the image. As described in Section 1.2, low spatial frequencies are associated with areas of relatively uniform signal intensity, whereas high spatial frequencies represent the fine detail within tissue, sharp boundaries between tissues, and also noise. A low-pass filter therefore improves the image SNR by attenuating the contribution from noise, but it also degrades the spatial resolution. Such a filter can be applied in the spatial domain via a convolution process, as shown in Figure 1.9. Convolution involves placing the filter kernel, in this case a 3×3 matrix, over the image pixels, multiplying each pixel by the corresponding component of the kernel, and replacing the center pixel by the average of these values. The kernel is then displaced by one pixel in the horizontal dimension, and the process is repeated until the kernel has been applied to all the pixels in this horizontal dimension. This process is repeated for the next row of pixels until the whole image has been filtered. Figure 1.9 shows three different simple image kernels for low-pass, high-pass, and edge-enhancing filters.

Figure 1.10 shows the effects of applying each of these three filters separately on different MRI brain scans. In practice, more sophisticated filtering is often performed, in which the filter has different characteristics for different areas of the image based on the local image characteristics: for example a Wiener filter provides an optimum trade-off between SNR and spatial resolution [9].

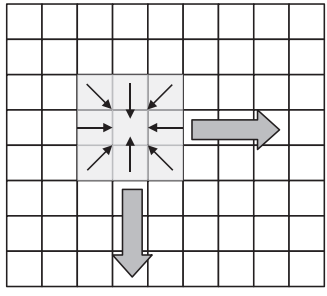

Low-pass	High-pass	Edge enhancing
1 1 1	−1 −1 −1	+1 +1 +1
1 4 1	−1 +9 −1	0 0 0
1 1 1	−1 −1 −1	−1 −1 −1

Figure 1.9 Illustration of how image convolution is carried out in the spatial domain. Three different 3×3 filter kernels are shown.

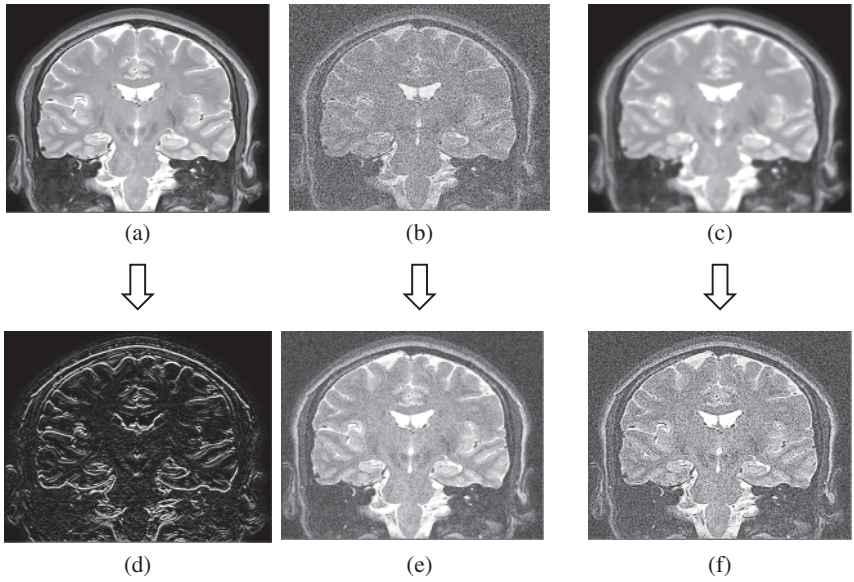

Figure 1.10 Illustrations of the effects of different post-acquisition filters. Transforming from image (a) to image (d) shows the effects of an edge-enhancing filter applied to a high-resolution, high SNR image. From image (b) to image (e) the effect of a low-pass filter on a noisy image. From image (c) to image (f) a high-pass filter applied to an image with low spatial resolution.

1.8 Assessing the Clinical Impact of Improvements in System Performance

The ultimate aim of improving the technology for medical imaging is of course to improve patient outcome. Fryback and Thornbury [10] have proposed six hierarchical levels to characterize the path from technological improvements to an increase in the clinical efficacy of diagnostic imaging: an adapted version is shown in Figure 1.11. It is important to note that there is not necessarily a straightforward correlation between technological development (level 1) and patient outcome efficacy (level 5). For example, a technical innovation may make a system much too expensive for widespread use: alternatively, the improvement may be deemed too small to change local medical insurance policies. In other words, traversing between different levels involves many more considerations than just the technical aspects of medical imaging which are considered in this book. Nevertheless, it is important to have a quantitative measure of, for example, how level 1 improvements in technology relate to level 2 improvements in diagnostic accuracy, sensitivity, and specificity, as covered in Section 1.8.1.

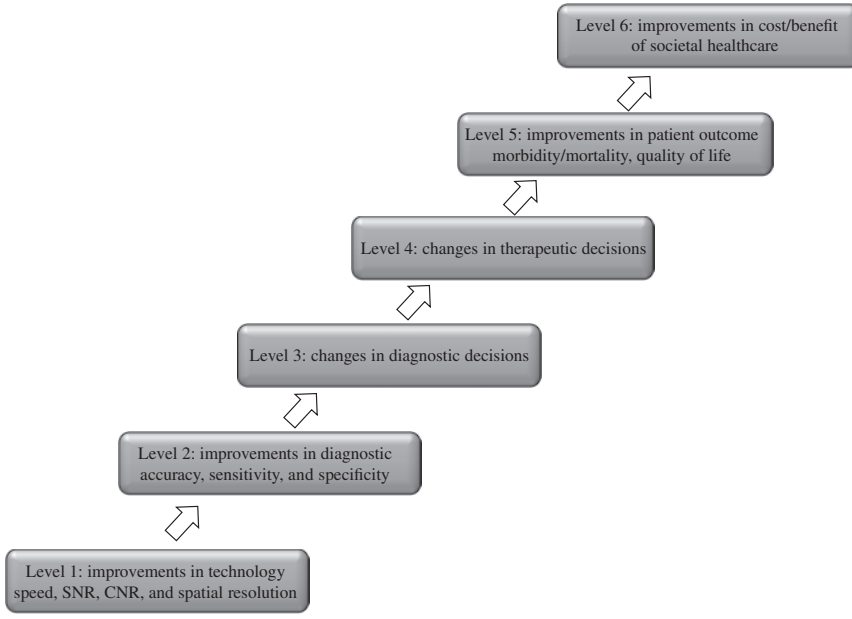

Figure 1.11 Levels of evidence in evaluating the efficacy of diagnostic imaging. Source: Adapted from Fryback and Thornbury [10].

1.8.1 The Receiver Operating Characteristic Curve

The quantitative effect of a technological improvement on clinical diagnosis can be assessed using a receiver operating characteristic (ROC) curve. The concept of the ROC curve is illustrated here with a simple example. Consider the situation in which a patient is suspected of having a tumor. There are four possibilities for a radiologist making the diagnosis based on a series of images: true positive (where true refers to the correct diagnosis and positive to the tumor being present), true negative, false positive, and false negative, as shown in Figure 1.12. Three measures are commonly used in ROC curve analysis:

Accuracy is the number of correct diagnoses divided by the total number of diagnoses,

Sensitivity is the number of true positives divided by the sum of the true positives and false negatives, and,

Specificity is the number of true negatives divided by the sum of the number of true negatives and false positives.

The ROC curve plots the sensitivity (also known as the true positive rate) on the vertical axis versus 1-specificity (also known as the false positive rate) on the horizontal axis. The area under the ROC curve is a measure of the effectiveness

	Actual situation	
Diagnosis	*Tumor present*	*Tumor absent*
Tumor present	True positive	False positive
Tumor absent	False negative	True negative

(a)

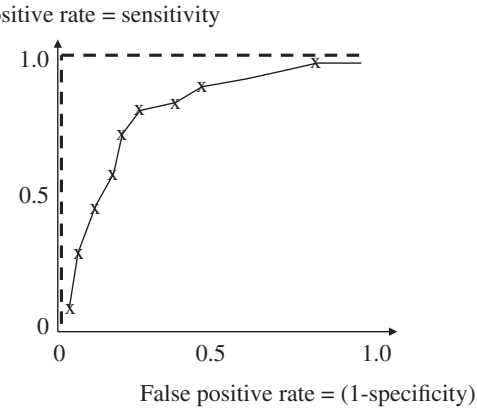

(b)

Figure 1.12 (a) A table showing the four possible outcomes of a tumor diagnosis. (b) An ROC curve corresponding to this table. The better the diagnosis, the higher the integrated area under the ROC curve. The dotted line shows the situation for a perfect diagnosis.

of the imaging system and/or the clinician's interpretation of the images. A value of 100% for accuracy, sensitivity, and specificity is represented by a point on the ROC curve given by a true-positive fraction of 1, and a false-positive fraction of 0, i.e. the dashed line in Figure 1.12. The closer the actual ROC curve lies to this ideal line, the better. The integral under the ROC curve, therefore, gives a quantitative measure of the quality of the diagnostic procedure. So, if the performance (SNR, CNR, and spatial resolution) of an imaging system is improved, an ROC curve analysis can be performed comparing the new versus the old system, with the result being a quantitative measure of the improvement in clinical quality.

1.A Appendix

1.A.1 Fourier Transforms

The Fourier transform is an integral part of image processing for many of the modalities covered in this book. For example, in MRI (Chapter 5), the signals are acquired in the spatial frequency domain, and the signals undergo a multi-dimensional inverse Fourier transform to produce the image. In ultrasound imaging (Chapter 4), spectral Doppler plots are the result of Fourier transformation of the time-domain demodulated Doppler signals. This short appendix summarizes the basic mathematics and useful properties of the Fourier transform.

1.A.2 Fourier Transforms of Time Domain and Spatial Frequency Domain Signals

The forward Fourier transform, $S(f)$, of a time domain signal, $s(t)$, is given by:

$$S(f) = \int_{-\infty}^{\infty} s(t)e^{-j2\pi ft}dt \tag{1.A.1}$$

The inverse Fourier transform, $s(t)$, of a frequency domain signal, $S(f)$, is given by:

$$s(t) = \frac{1}{2\pi}\int_{-\infty}^{\infty} S(f)e^{+j2\pi ft}df \tag{1.A.2}$$

The forward Fourier transform, $S(k)$, of a spatial domain signal, $s(x)$, is given by:

$$S(k) = \int_{-\infty}^{\infty} s(x)e^{-j2\pi k_x x}dx \tag{1.A.3}$$

The corresponding inverse Fourier transform, $s(x)$, of a spatial frequency domain signal, $S(k)$, is given by:

$$s(x) = \int_{-\infty}^{\infty} S(k)e^{+j2\pi k_x x}dk \tag{1.A.4}$$

Some useful Fourier pairs are shown in Figure 1.A.1.

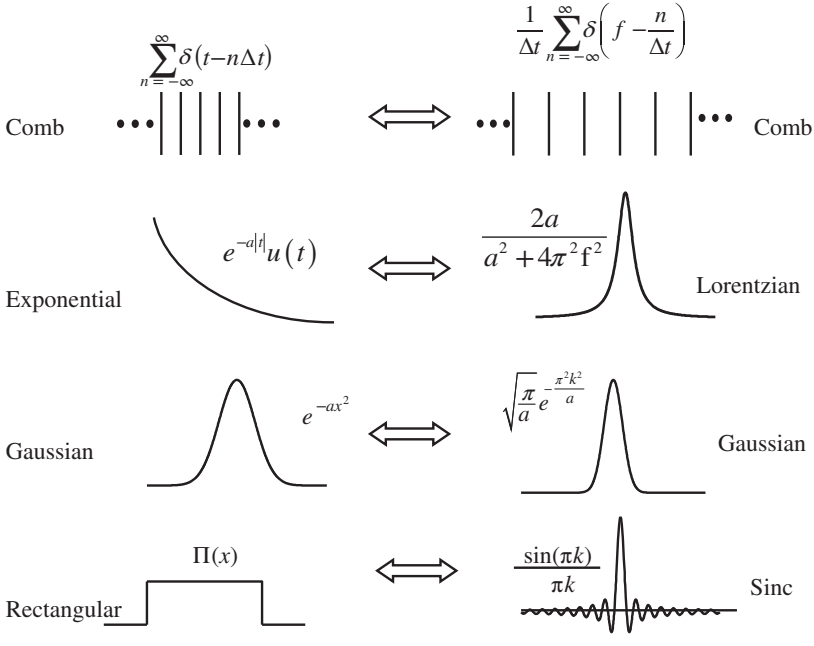

Figure 1.A.1 Some Fourier transform pairs commonly used in imaging.

Imaging signals are acquired in more than one dimension, and image reconstruction then requires multi-dimensional Fourier transformation. For example:

$$S(k_x, k_y) = \int_{-\infty}^{\infty} \int_{-\infty}^{\infty} s(x, y) e^{-j2\pi(k_x x + k_y y)} dx dy \tag{1.A.5}$$

$$s(x, y) = \int_{-\infty}^{\infty} \int_{-\infty}^{\infty} S(k_x, k_y) e^{+j2\pi(k_x x + k_y y)} dk_x dk_y \tag{1.A.6}$$

and similarly, in three dimensions. Highly efficient computational algorithms make the Fourier transform one of the quickest mathematical transforms to perform.

1.A.3 Useful Properties of the Fourier Transform

In order to understand many aspects of medical imaging, both in terms of the spatial resolution inherent to the particular modality and also the effects of image post-processing, a number of mathematical properties of the Fourier transform are very useful. The most relevant examples are listed below

(a) Linearity: The Fourier transform of two additive functions is itself additive:

$$a\mathrm{s}_1(t) + b\mathrm{s}_2(t) \Leftrightarrow a\mathrm{S}_1(f) + b\mathrm{S}_2(f)$$

$$a\mathrm{S}_1(x) + b\mathrm{S}_2(x) \Leftrightarrow a\mathrm{s}_1(k_x) + b\mathrm{s}_2(k_x) \tag{1.A.7}$$

This theorem shows that if the acquired time-domain signal consists of, for example, the sum of a number of different sinusoidal functions, each with a different frequency and amplitude, then the relative amplitudes of each component are maintained when the data are Fourier transformed, as shown in Figure 1.A.2.

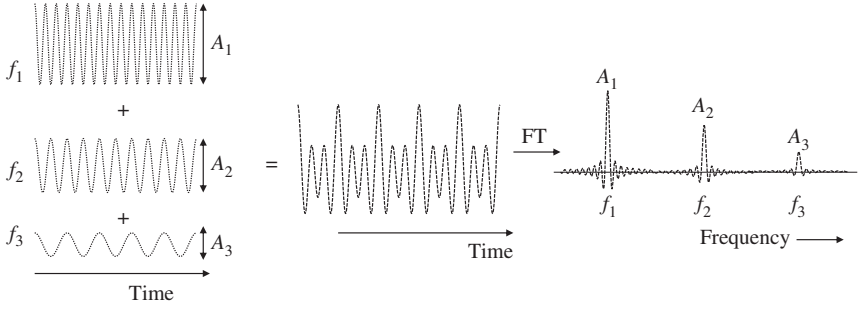

Figure 1.A.2 Illustration of the linearity of the Fourier transform. A time-domain signal (middle) is composed of three different time-domain signals (left). The Fourier transformed frequency spectrum (right) consists of signals from each of the three different frequencies with the same amplitudes as in the time-domain data.

(b) Convolution: The equivalent of multiplying two signals together in the time domain is the convolution (*) of the two individual Fourier transformed components in the spatial frequency domain, and vice versa:

$$s_1(t)s_2(t) \Leftrightarrow S_1(f) * S_2(f)$$

$$s_1(k_x)s_2(k_x) \Leftrightarrow S_1(x) * S_2(x) \tag{1.A.8}$$

The convolution of two functions $p(x)$ and $q(x)$ is defined as:

$$p(x) * q(x) = \int_{-\infty}^{\infty} p(x-\tau)q(\tau)d\tau \tag{1.A.9}$$

(c) Scaling law: if either a time-domain or spatial-domain signal is scaled by a factor b, then its Fourier transform is scaled by the inverse factor $1/b$, i.e.:

$$s(bt) \Leftrightarrow \frac{1}{|b|}S\left(\frac{f}{b}\right)$$

$$s(bx) \Leftrightarrow \frac{1}{|b|}S\left(\frac{k_x}{b}\right) \tag{1.A.10}$$

One example already encountered in Section 1.3.3 is the correspondence of a narrow PSF to a broad MTF, and vice versa.

Exercises

Section 1.2

1.1 For the one-dimensional objects $O(x)$, and LSFs $h(x)$ shown in Figure 1.13, draw the resulting projections $I(x)$. Write down whether each object contains high spatial frequencies, low spatial frequencies, or both. Which image best represents the object, and which is the most distorted?

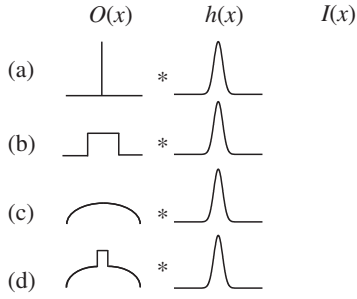

Figure 1.13 Exercise to show the effect of a fixed $h(x)$ on four different objects $O(x)$.

Section 1.3

1.2 Show mathematically that the FWHM of a Gaussian function is given by:

$$\text{FWHM} = \left(2\sqrt{2\ln 2}\right)\sigma \cong 2.36\sigma$$

1.3 Plot the MTF on a single graph for each of the convolution filters shown below (Figure 1.14).

1	1	1
1	4	1
1	1	1

1	1	1
1	12	1
1	1	1

1	1	1
1	1	1
1	1	1

Figure 1.14 Exercise to calculate the MTF associated with three different convolution kernels.

Section 1.4

1.4 If the ROI chosen for an estimate of the SNR is four times bigger than the ROI chosen to estimate the standard deviation of the background noise, how does this affect the SNR measurement?

1.5 If the SNR is very low, then the formula given by equation (1.7) is no longer valid. Explain why this is so, and suggest what corrections could be made in this case.

Section 1.6

1.6 An analog signal of 526.35 mV is to be digitized using (i) a four-bit, (ii) a six-bit, and (iii) an eight-bit ADC, each with a voltage range of 1 V. Calculate the digitized signals for the three cases, and the percentage error compared to the actual analog signal.

1.7 Explain the effects of a signal which has a magnitude higher than the upper limit of an ADC. What does the time-domain signal look like, and what effect does this have on the frequency-domain signal?

1.8 An ultrasound signal is digitized using a 16-bit ADC at a sampling rate of 3 MHz. If the image takes 20 ms to acquire, how much data (in Mbytes) are there in each ultrasound image. If images are acquired for 20 s continuously, what is the total data output of the scan?

1.9 If a signal is digitized at a sampling rate of 20 kHz, at what frequency would a signal at 22 kHz appear?

1.10 A signal is sampled every 1 ms for 20 ms, with the following actual values of the analogue voltage at successive sampling times. Plot the values of the voltage recorded by a 5 V, 2-bit ADC assuming that the noise level is much lower than the signal and so can be neglected. On the same graph, plot the quantization error.

$$\text{Signal (volts)} = -4.3, +1.2, -0.6, -0.9, +3.4, -2.7, +4.3, +0.1, -3.2, -4.6, + 1.8, +3.6, +2.4, -2.7, +0.5, -0.5, -3.7, +2.1, -4.1, -0.4$$

1.11 Using the same signal as in Exercise 1.10, plot the values of the voltage and the quantization error recorded by a 5 V, 3-bit ADC.

Section 1.8

1.12 In a patient study for a new test for multiple sclerosis (MS), thirty-two of the one hundred patients studied actually have MS. For the data given below, complete the two-by-two matrices and construct an ROC. The number of lesions detected in each patient corresponds to the threshold value for designating MS as the diagnosis.

No. lesions detected	50	40	30	20	10	5	2
	2 | 0	8 | 1	16 | 3	22 | 6	25 | 15	30 | 35	32 | 60

1.13 Choose a medical condition and suggest a clinical test which would have:
(a) High sensitivity but low specificity,
(b) Low sensitivity but high specificity.

1.14 What does an ROC curve that lies below the random line, i.e. a line at 45° in Figure 1.12(b), suggest? Could this be diagnostically useful?

References

1 F. R. Verdun, D. Racine, J. G. Ott, M. J. Tapiovaara, P. Toroi, F. O. Bochud, W. J. H. Veldkamp, A. Schegerer, R. W. Bouwman, I. H. Giron, N. W. Marshall, and S. Edyvean, Image quality in CT: from physical measurements to model observers, *Physica Med.* 31(8):823–843 (2015).

2 S. D. Yu, G. Z. Dai, Z. Y. Wang, L. D. Li, X. H. Wei, and Y. Xie, A consistency evaluation of signal-to-noise ratio in the quality assessment of human brain magnetic resonance images, *BMC Med. Imaging* 18, 17 (2018).
3 K. M. Kempski, M. T. Graham, M. R. Gubbi, T. Palmer, and M. A. L. Bell, Application of the generalized contrast-to-noise ratio to assess photoacoustic image quality, *Biomed. Opt. Express* 11(7):3684–3698 (2020).
4 A. Rodriguez-Molares, O. M. H. Rindal, J. D'hooge, S. E. Masoy, A. Austeng, M. A. L. Bell, and H. Torp, The generalized contrast-to-noise ratio: a formal definition for lesion detectability, *IEEE Trans. Ultrason. Ferroelectr. Freq. Control* 67(4):745–759(2020).
5 J. H. Yan, J. Schaefferkoetter, M. Conti, and D. Townsend, A method to assess image quality for low-dose PET: analysis of SNR, CNR, bias and image noise, *Cancer Imaging* 16, 26 (2016).
6 A. Ng and J. Swanevelder, Resolution in ultrasound imaging, *Continuing Educ. Anaesth. Criti. Care Pain* 11(5):186–192 (2011).
7 W. W. Moses, Fundamental limits of spatial resolution in PET, *Nucl. Instrum. Methods Phys. Res., Sect. A* 648 Supplement 1:S236–S240 (2011).
8 L. Rayleigh, Investigations in optics, with special reference to the spectroscope, *Philos. Mag.* 8 (49), 261–274 (1879).
9 Y. Q. Zeng, B. C. Zhang, W. Z. hao, S. X. Xiao, G. K. Zhang, H. P. Ren, W. B. Zhao, Y. H. Peng, Y. T. Xiao, Y. W. Lu, Y. S. Zong, and Y. M. Ding, Magnetic resonance image denoising algorithm based on cartoon, texture, and residual parts, *Comput. Math. Methods Med.* 2020, 1405647 (2020).
10 D. G. Fryback and J. R. Thornbury, The efficacy of diagnostic-imaging, *Med. Decis. Making* 11(2):88–94 (1991).

Further Reading

Books

J. Prince and J. Links, *Medical Imaging Signals and Systems*, 2nd ed., Pearson, New York City, USA (2014).
H. Azhari, J. A. Kennedy, N. Weiss, and L. Volokh, *From Signals to Image: A Basic Course on Medical Imaging for Engineers*, Springer, Cham, Switzerland (2020).

Review Articles

A. Kayugawa, M. Ohkubo, and S. Wada, Accurate determination of CT point-spread-function with high precision, *J. Appl. Clin. Med. Phys.* 14 (4):216–226 (2013).
L. Z. Chow and R. Paramesran, Review of medical image quality assessment, *Biomed. Signal Process. Control* 27, 145 (2016).

A. N. Kamarudin, T. Cox, and R. Kolamunnage-Dona, Time-dependent ROC curve analysis in medical research: current methods and applications, *BMC Med. Res. Method.* 17, 53 (2017).

N. A. Obuchowski and J. A. Bullen, Receiver operating characteristic (ROC) curves: review of methods with applications in diagnostic medicine, *Phys. Med. Biol.* 63, 07TR01 (2018).

S. Perfetto, J. Wilder, and D. B. Walther, Effects of spatial frequency filtering choices on the perception of filtered images, *Vision* 4, 4020029 (2020).